



CHAPTER V

BIO-NANOCOMPOSITE SYSTEM OF NANO-CHITOSAN IN EPOXIDIZED NATURAL RUBBER

5.1 Abstract

Bio-nanocomposite systems of epoxidized natural rubber and nano-sized chitosans in nanoscaffold form (CSN) and nanofibrous form (RCS) are considered. The morphology of ENR nanocomposites was studied by TEM showing the dispersion of biofillers in ENR matrices. Both nano-sized chitosans bring the roughness and stiffness on the ENR surface as observed by SEM and AFM. SEM metal ion mapping mode also demonstrates the copper ion adsorptivity on the bio-nanocomposites. At the appropriate biofillers content above 10 phr, the crosslink density, swelling, hardness, and mechanical properties are improved.

Keywords: Chitin-chitosan; Epoxidized natural rubber; Bio-nanocomposite; Nanoscaffold; Nanofiber

5.2 Introduction

Compounding natural rubber with additives to achieve physical and mechanical properties is known as a way to manufacture the value-added products. The properties of rubber can be tailored by adding fillers and additives of which the interaction based on the hydrophobicity/hydrophilicity, morphology, aggregation, and aspect ratio (in the case of fibers)¹⁻³, plays an important role in developing physical and mechanical properties to the rubber products. Carbon black and silica are recognized as the main fillers to improve physical and mechanical properties of the rubber.^{4,5}

Although the carbon black satisfies the applications, especially for tires, the fact that the black color limits the variable appearances whereas the production of carbon black involves with health safety and the combustion of rubber with carbon black generating smokes and carbon mono- and dioxide pollution. Silica is good in

terms of colors and mechanical strength, although the high density brings the heavy weight to the rubber products. Considering the waste treatment after use of rubber products, especially tires, the landfill and pyrolysis are only choices which life cycle assessment is still an issue.⁶

Based on this viewpoint, the renewable resources based fillers; especially natural fibers have received much attention in the current years.^{2,3,7-11} The advantages of natural fiber are not only for its green materials, but also its high strength and toughness based on the fiber packing structure and high aspect ratio, including its low density which gives the product the light weight¹², and the simple filler preparation^{2,7} which related to the reasonable price. Up to present, composite materials with natural fibers have been variously reported.

Recently, Nair and Dufresne have proposed the use of chitin biofiller in rubber. They demonstrated the preparation of nano-whiskered chitin and the simple system of natural rubber (NR) /chitin whisker, by which the physical and mechanical properties were, improved.^{2,3} There, the reinforced rubber with chitin whisker was reported to be dependent on the rigid three-dimensional network formation and the high specific surface area.¹³

Recently, our group succeeded in preparing chitosan nanoscaffold by simply extending the deacetylation of chitin whisker.^{14,15} This material is attractive in term of the fibrous network morphology. Here, the use of nanoscaled chitosan as fillers for rubber bio-nanocomposite is focused. Considering the rubber, it has to be accepted that the epoxidized natural rubber (ENR) is more hydrophilic as compared to NR. Thus, it provides hydrophilic composite matrices for chitosan as compared to NR. The extent of epoxidation unit gives an increase of polarity and glass transition temperature.^{1,16-18} The increase in polarity is important when one considers the reinforcement by polar fillers with a good interaction between fillers and polymer matrices.¹⁹

The present work, thus, focuses on the bio-nanocomposite system of nano-sized chitosan and ENR. Here, two types of nano-chitosan with different morphologies, i.e., nanoscaffold and nanofibrous chitosan, are applied as nano-additives to obtain ENR bio-nanocomposite materials.

5.3 Experimental

5.3.1 Materials

Chitosan flake with a percent degree of deacetylation (%DD) of 95 and chitin from shrimp shell were provided by Seafresh (Lab) Company Limited, Thailand. Epoxidized natural rubber (ENR) latex was supplied from Sumirubber Malaysia SDN. BHD., Malaysia. Sodium hydroxide (NaOH) was purchased from Fluka Chemicals, Switzerland. Hydrochloric acid (HCl) and acetic acid were from Carlo Erba, Italy. Sulfur (S), zinc oxide (ZnO), stearic acid, and *N*-cyclohexyl-2-benzothiazyl sulphenamide (CBS) were the gifts from the Research and Development Center for Thai Rubber Industry, Mahidol University, Thailand. All chemicals were AR grade and used without further purification.

5.3.2 Instruments and equipment

Proton nuclear magnetic resonance ($^1\text{H-NMR}$) spectra were collected from a Bruker Avance 400 spectrometer with 512 scans by using $\text{CD}_3\text{COOD}/\text{D}_2\text{O}$ (2 % v/v) as a solvent. Wide angle X-ray diffraction (WAXD) patterns were obtained over a 2 to 60° 2θ range by a RIGAKU RINT 2000 using $\text{Cu K}\alpha$ as an X-ray source equipped with a Ni filter and operating at 40 kV and 30 mA.

The ENR composites were compounded by using a two-roll mills machine (Labtech, Thailand). The compound was vulcanized by using a Vantage of compression moulding (WABASH, USA).

The cure characteristics were determined by using a Rheotch MD+ moving die rheometer (MDR) (TECHPRO, USA). The hardness properties were evaluated by a Shore A Durometer (Zwick Materialprüfung Durometer, Germany). Tensile properties were measured by using an INSTRON 5566 of universal testing machine (INSTRON, USA). The density was determined by using an Ultrapycnometer 1000 (Quantachrome instruments, USA). Thermogravimetric analyses were observed by using a Perkin–Elmer Pyris Diamond TG-DTA (Connecticut, USA) with N_2 flow rate of 20 mL/min at the temperature starting from 50 to 500 °C. Thermal evaluation

was operated with the heating rate of 10 °C/min. The morphology was observed by a H-1700 transmission electron microscopy (TEM) (Hitachi-High-Technology Corporation, Japan) at 100 kV and a S-4800 field emission scanning electron microscope (FE-SEM) (Hitachi-High-Technology Corporation, Japan). The nano-chitosan distribution was analyzed by energy dispersion X-ray (EDX) detector (EMAX X-act, HORIBA, attached to the S-4800 SEM) for evaluating Cu²⁺ on chitosan. Atomic force microscopy (AFM) measurements were carried out by using a XE-100 AFM (Park systems corporation, Korea) connected with NSC36 silicon cantilever coating with Al in the force modulation microscopy (FMM) mode in air at room temperature.

5.3.3 Preparation of chitosan nanoscaffold (CSN)

The preparation of chitosan nanoscaffold was carried out according to our previous report.¹⁴ In brief, chitin whisker (5 mL) was deacetylated by 50 % NaOH solution (w/v) 25 mL at 150 °C for 21 h. The solution obtained was centrifuged and the precipitates were collected and washing with distilled water until neutral to obtain CSN.

5.3.3 Preparation of reprecipitated chitosan (RCS)

Chitosan flake (1g) was dissolved in 2 % (v/v) acetic acid 100 mL to obtain chitosan solution. The reprecipitated chitosan was obtained by a slow reprecipitation of chitosan solution in 1 % (w/v) NaOH solution. The crude product was washed thoroughly with distilled water to obtain RCS.

5.3.3 Preparation of ENR nanocomposites

Preparation of ENR nanocomposites. The solutions of CSN and RCS were concentrated to the paste form to find the solid content of 6.25 and 5.38 %, respectively. The paste was mixed with ENR latex with the content of 2.5, 5, 10, and 20 phr of ENR content. Each mixture was cast on a plastic plate and dried in oven at

60 °C to obtain the dry sheets. The sheets obtained are further formulated on a two roll mill at 40 °C with 3, 1.5, 1, and 2 phr of ZnO, S, CBS, and stearic acid, respectively. Then, vulcanization was carried out on a compression molding at 150 °C for the optimum cure time (t_{90}).

Swelling degree. Swelling degree of the vulcanized rubber was performed in toluene and methanol for 24 h at room temperature. Then, the swelling percentage was calculated based on eq (1).20

$$\text{Swelling percentage} = \left(\frac{W_s - W_i}{W_i} \right) \times 100 \% \quad \text{eq. (1)}$$

W_i and W_s are the original weight of sample and the weight of sample after immersing in toluene and methanol for 24 h, respectively, obtained from TG-DTA.

Crosslink density measurement. The vulcanized rubbers were evaluated the crosslink density by using Flory-Rehner equation (eq. (2)) 21,22:

$$\eta_{phys} = \frac{-\left[\ln(1 - \Phi_r) + \Phi_r + \chi \Phi_r^2 \right]}{V_o \left[\Phi_r^{1/3} - \frac{\Phi_r}{2} \right]}, \quad \text{eq. (2)}$$

where η_{phys} is the degree of crosslink density (mol/cm³), V_o is the molar volume of toluene (106.3 cm³/mol), and χ is Flory-Huggins interaction parameter between toluene and rubber (0.393). Φ_r is the volume fraction of rubber, which was calculated by eq. (3):

$$\frac{1}{\Phi_r} = 1 + \frac{W_s \rho_r}{W_i \rho_s}, \quad \text{eq. (3)}$$

where ρ_r and ρ_s are densities of rubber compound (g/cm³) and toluene (0.87 g/cm³), respectively. W_i and W_s are the weights of dry rubber and swollen rubber (g), respectively.

5.4 Results and discussion

5.4.1 Chemical characterization

Nair and Dufresne reported that the specific acid treatment condition bring chitin flakes to chitin whiskers.² In general, the alkaline treatment changes chitin to chitosan.²³ Here, chitin whisker was used as a starting material to deacetylate to chitosan. The degree of deacetylation was confirmed by ¹H-NMR to find that it was as high as 97 %.²⁴ At that time, as reported in the past, chitin in whisker form was changed to chitosan in network or nanoscaffold form (CSN) with diameter in the range of 40-75 nm as shown in Figure 5.1a.

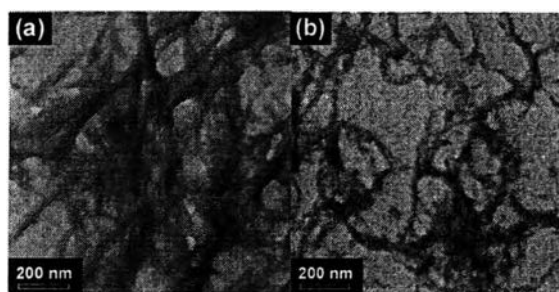


Figure 5.1. TEM micrographs of (a) CSN and (b) RCS.

At the same time, the reprecipitated chitosan was also prepared directly from chitosan flakes. The reprecipitation of chitosan-acetic acid solution in alkaline solution brings the reprecipitated chitosan (RCS) in random nanofiber form having diameter in the range of 30-70 nm as confirmed by TEM (Figure 5.1b). At that time, the degree of deacetylation of the RCS was 90 % as confirmed by ¹H-NMR.²⁵

5.4.2 Morphological studies of bio-nanocomposites

In order to control the amount of CSN and RCS, the paste forms of both chitosans were dried up. It should be noted that the dry solid contents of CSN and RCS were 6.25 and 5.38 %, respectively. Thus, in the bio-nanocomposite preparation, the amount of chitosans was based on the dry solid content amount to control the equal amount in phr.

After ENR was incorporated with CSN and RCS, the dispersion of the nanocomposite was observed by TEM. Figure 5.2a show the TEM of a typical ENR sheet without any chitosan. As the samples have to be sheared by cryogenic microtome, the transparent part implied the tiny hole in the sample. The dark spots

all over the sample are the ZnO. Based on the ENR sheet, the ENR blending with CSN (Figure 5.2b) and the ENR blends with RCS (Figure 5.2c) can be discussed as follows. In the case of ENR blending with CSN, the nanocomposite system shows the dark layers which might refer to CSN bio-additive parts appearing all over the sample implying the existence and the distribution of CSN. It is important to note that there are some transparent traces which might be the thin areas or the open areas. This reflects the pilling off of CSN during microtome shear in sample preparation step. Although many samples were neatly prepared, the similar TEM micrographs were observed.

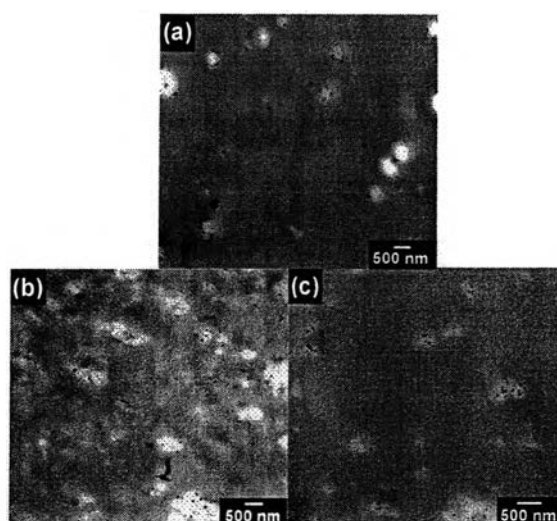


Figure 5.2. TEM micrographs of (a) ENR and ENR nanocomposites with CSN (b) and RCS (c) at 20 phr.

For RCS, the significant white areas appear throughout the sample. When the content is 20 phr, some dark areas can be observed as shown in Figure 5.2c. This implied that the RCS almost completely pilled out from the sample during the microtome abrasion.

The fact that CSN is still remained in the TEM sample whereas RCS was almost pilled out from the sample, we suspect that the interaction of CSN and ENR might be strong enough to allow the CSN maintained in the sample even the microtome abrasion (*more discussion in Tensile fracture surface feature*).

5.4.3 Surface characterization by AFM

In order to evaluate the effect of nano-sized chitosan on the surface property of ENR, the coating of NR latex on both ENR and ENR nanocomposites surfaces was used as a reference. Atomic force microscopy (AFM) was applied by using a force modulation microscopy (FMM) mode. Figure 5.3 displays topographic images and profiles of NR/ENR and NR/ENR nanocomposite surfaces, which are generated from the contact between the tip and sample surface.²⁶⁻²⁸ ENR incorporating with nano-sized chitosan displays the rough surface as compared to the pure ENR. This implies that the nano-sized chitosan induces the roughness on ENR surface. Figure 5.4 shows the FMM amplitude images and profiles of NR/ENR and NR/ENR nanocomposite with nano-sized chitosan. FMM amplitude image (Figure 5.4A) and signal in amplitude profile (Figure 5.4B) of the pure ENR surface are similar to those of NR indicating that the ENR surface has the surface property in line with NR.²⁶ However, ENR nanocomposites show the light images (Figures 5.4A(b)- 5.4A(e)) and the high amplitude signals (Figures 5.4B(b)- 5.4B(e)) as compared to ENR. This implies that CSN brings stiffness onto ENR surface. Jourdan et al. reported that the different in viscoelastic properties of the surface caused the different in amplitude and phase²⁹, thus, FMM phase was also considered. FMM phase image of pure ENR (Figure 5.5A(a)) demonstrates the same image as that of NR, whereas, FMM phase profile of pure ENR shows higher signal than that of NR. Considering ENR incorporating with CSN at 20 phr (Figure 5.5B(e)), FMM phase signal displays lower signal as compared to ENR. This suggests that CSN causes the stiffness of ENR surface.³⁰ The changes in surface stiffness was also evaluated by using the plot of relative FMM amplitudes and FMM phases using NR as a reference with nano-sized chitosan contents (Figure 5.6). Both CSN and RCS show an increase in FMM amplitude and the decrease in FMM phase with an increase of chitosan contents.

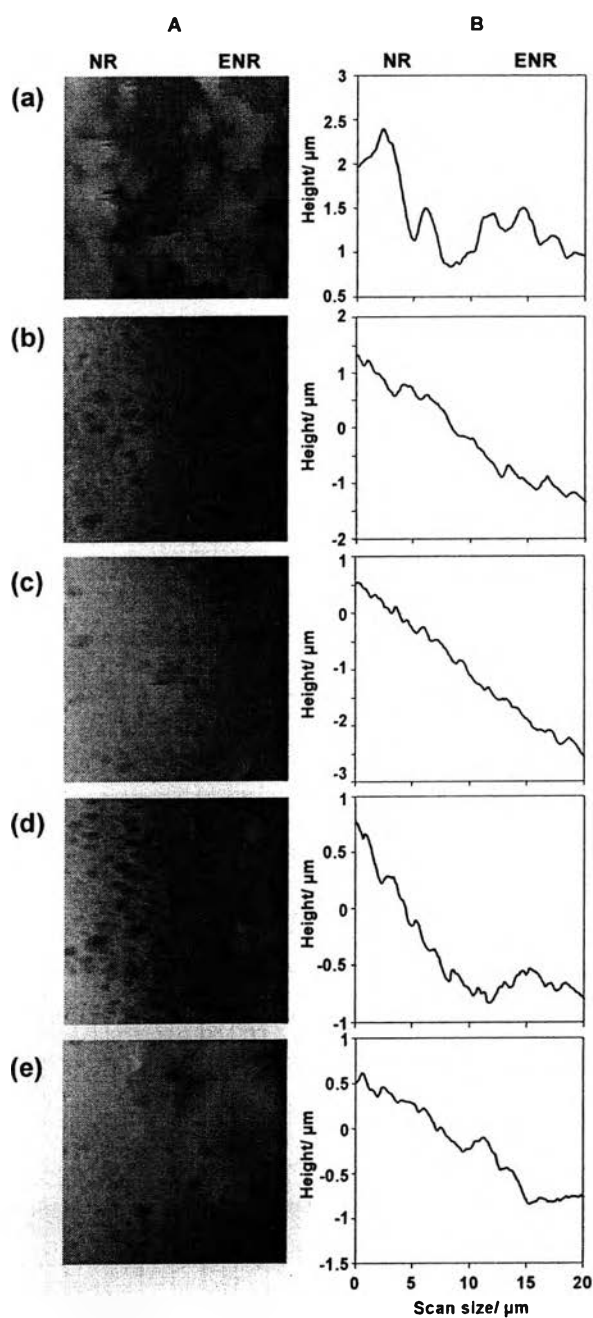


Figure 5.3. (A) Topographic images and (B) topographic profiles of ENR (a) and ENR incorporating with CSN at 2.5 (b), 5 (c), 10 (d), and 20 phr (e) in the size of 20 μm^2 .

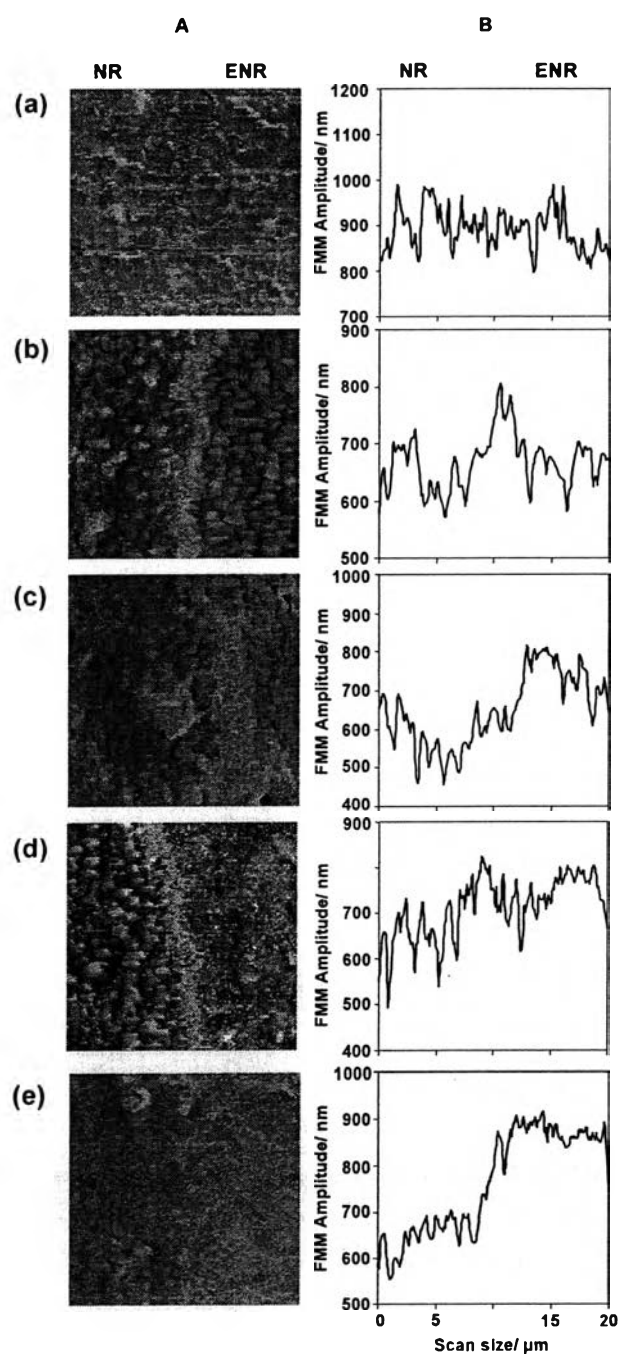


Figure 5.4. (A) FMM amplitude images and (B) FMM amplitude profiles of ENR (a) and ENR incorporating with CSN at 2.5 (b), 5 (c), 10 (d), and 20 phr (e) in the size of $20 \mu\text{m}^2$.

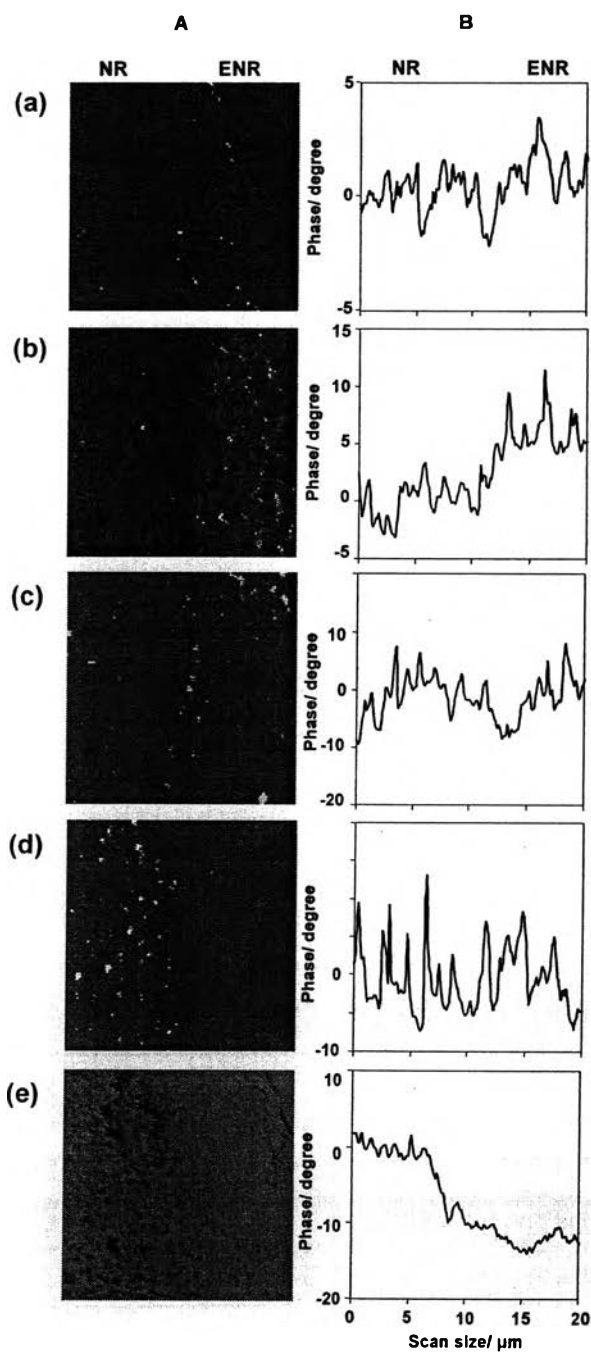


Figure 5.5. (A) Phase images and (B) phase profiles of ENR (a) and ENR incorporating with CSN at 2.5 (b), 5 (c), 10 (d), and 20 phr (e) in the size of $20 \mu\text{m}^2$.

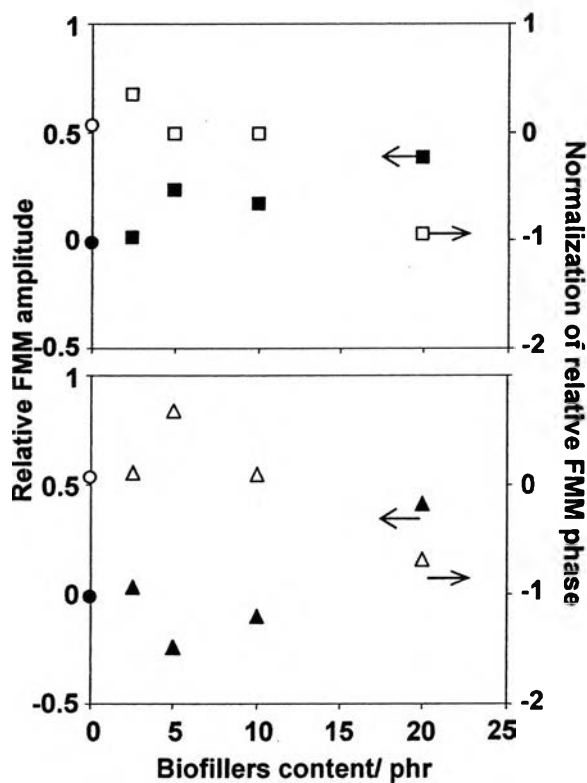


Figure 5.6. Relative FMM amplitude (solid) and normalization of FMM phase (blank) of ENR (●) and ENR nanocomposites with CSN (■) and RCS (▲) at various biofillers contents.

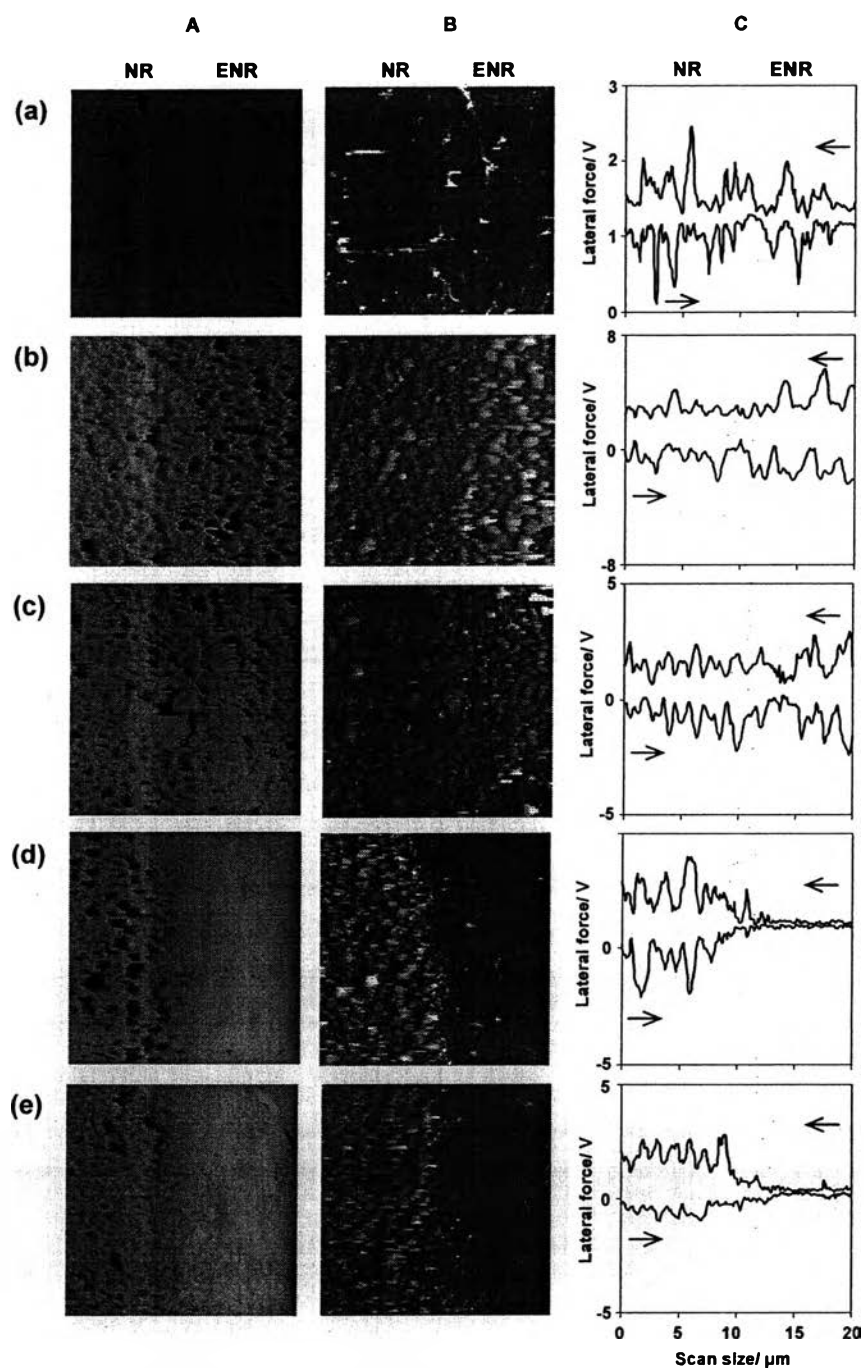


Figure 5.7. (A) Lateral force images (forward), (B) Lateral force images (backward), and (C) lateral force loop of ENR (a) and ENR incorporating with CSN at 2.5 (b), 5 (c), 10 (d), and 20 phr (e) in the size of $20 \mu\text{m}^2$.

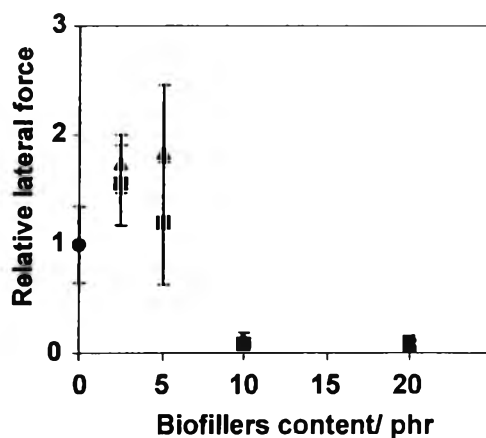


Figure 5.8. Relative FMM lateral force of ENR (●) and ENR nanocomposites with CSN (■) and RCS (▲) at various biofillers contents.

Taking the lateral force into the consideration, lateral force is generated by the tip deflection or friction force between tip and sample surface.³¹ Figure 5.7 demonstrates the forward and backward lateral force images and lateral force loop signals of ENR and ENR nanocomposites with CSN. The NR layer shows the smooth surface in lateral force images rather than the pure ENR surface (Figure 5.7A(a) and 5.7B(a)). The lateral force signal also demonstrates the lower value than the pure ENR. It means that the friction force of ENR surface has higher than NR surface. Considering ENR incorporating with CSN, the ENR nanocomposites surfaces display the smoother surface when CSN content increases (Figure 5.7A and 5.7B). The lateral force loop also decreases with CSN contents as compared to the NR reference surface. In order to clearly evaluate the lateral force, the relative lateral force was determined by the ratio of lateral force loop between ENR nanocomposites and NR layer. The relative lateral force is plotted with biofillers content as shown in Figure 5.8. Both nano-chitosans induce the decrease in lateral force on the ENR nanocomposites surface in the same level as function with chitosan content indicating that the decrease in friction force between tip and sample surface is attributed to the nano-chitosan in ENR matrices.

5.4.4 Surface analysis of bio-nanocomposites adsorption with Cu^{2+}

The surface morphology was also further clarified by using FE-SEM technique. Figure 5.9a displays the smooth surface of the pure ENR, while Figures 5.9b and 5.9c show the rough surface of ENR incorporating with CSN and RCS. This result is related to that of the topographic images from AFM. This proves that the nano-sized chitosan induce the roughness on the ENR surface. It is important to note that the amino group of chitosan has the unique property to complex with various metal ions such as Cu^{2+} , Cd^{2+} , Ni^{2+} , Fe^{2+} , Fe^{3+} , Zn^{2+} , and Hg^{2+} .^{32,33} Considering the complexation ability of nano-chitosans, after nano-chitosans were functioned in ENR matrices as reinforcing agent, the amino groups of chitosan also maintained their unique property with metal ions. Bio-nanocomposites were immersed in the copper sulfate solution in order to adsorb metal ions.

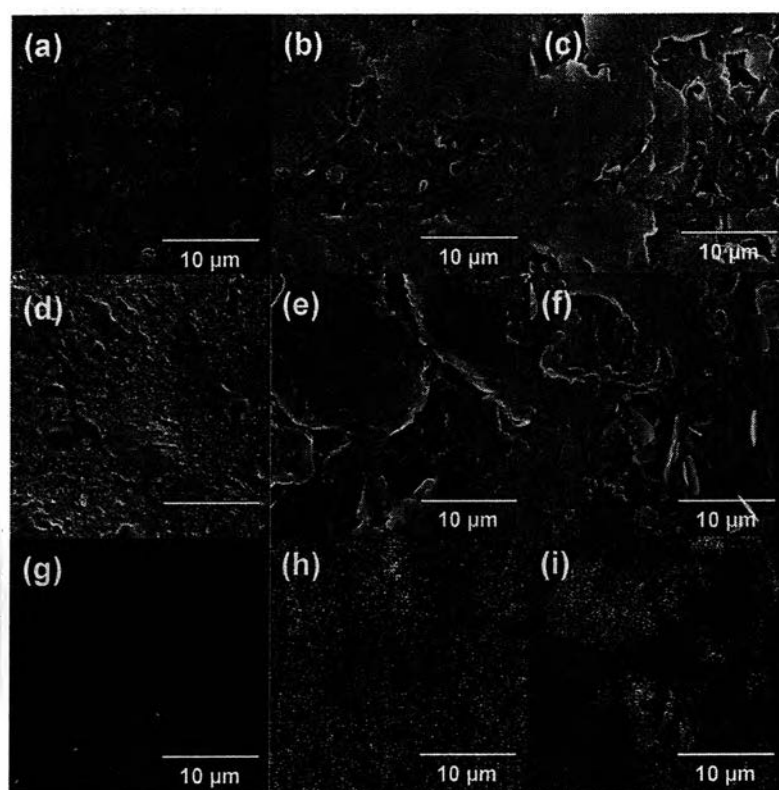


Figure 5.9. FE-SEM surface micrographs of (a) ENR and ENR incorporating with (b) CSN and (c) RCS at 20 phr, after immersing in copper solution of (d) ENR and ENR incorporating with (e) CSN and (f) RCS at 20 phr and copper mapping mode of (g) ENR and ENR incorporating with (h) CSN and (i) RCS at 20 phr.

Figures 5.9d-5.9f display the surface morphologies after immersing in copper sulfate solution of ENR and ENR nanocomposite with CSN and RCS by using copper ion FE-SEM mapping mode. The copper mapping results not only inform the metal adsorbability on chitosan but also report to the chitosan distribution in ENR matrices. In the case of ENR/CSN nanocomposites system (Figure 5.9h), the Cu^{2+} ions disperse all over the ENR matrix as compared to the pure ENR (Figure 5.9g). This suggests that CSN biofillers are good distribution in ENR matrix. Figure 5.9i shows the agglomeration of Cu^{2+} ions in ENR/RCS nanocomposites. This informs that the agglomerated RCS is presented in ENR matrices. This result suggests that the dispersion of CSN is better than that of RCS in ENR matrices.

5.4.5 Cure characteristics

In order to identify the cure characteristics of ENR and ENR nanocomposites, the maximum and minimum torque (M_H and M_L) were evaluated. In general the torque minimum (M_L) implies the viscosity of the material²¹, whereas the torque maximum (M_H) refers to viscosity of the material after curing. The differences, i.e., $M_H - M_L$, are referred to the crosslink density.

Figure 5.10 shows the M_H , and ($M_H - M_L$) between ENR and ENR nanocomposites with either CSN or RCS. In the case of ENR, the M_H and M_L are 4.69 and 0.18 dNm, respectively. The crosslink density, therefore, is 96 %. For ENR nanocomposites with CSN 2.5 and 5 phr, the torque values are about 75 % to that of ENR. The decreases in torque and the crosslink density might come from the fact about the decrease in content of ENR, and as a consequence, the less crosslink. When the CSN content was above 10 phr, the torque is increased implying the toughness of the rubber. In other words, the 10 phr of CSN content is high enough to function as a reinforcing network to ENR matrices.

Based on the ENR, ENR nanocomposites with RCS in the content from 2.5 to 10 phr show the decrease in crosslink density. This is relevant to the crosslink density results of ENR/CSN nanocomposites. Although the interaction with ENR matrices might not be high enough to give good miscibility as resulted in TEM

(Figure 5.2), the crosslink density at 20 phr of RCS content is also significant. This suggests that the RCS acts as reinforcing network to ENR matrices at 20 phr.

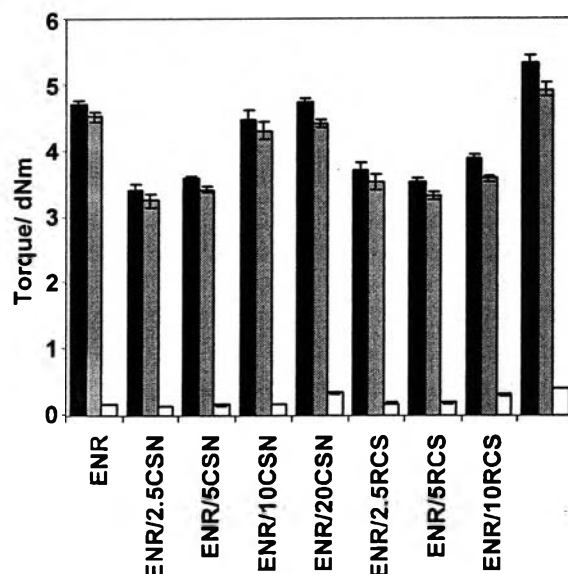


Figure 5.10. Torque maximum (M_H , ■), torque minimum (M_L , □), and torque difference ($M_H - M_L$, ▨) of ENR and ENR nanocomposites.

5.4.6 Crosslink density

The crosslink density of ENR nanocomposites was determined by Flory-Rehner (eq. (2)). Table 5.1 shows the change in crosslink density of ENR nanocomposites. The results are relevant to what obtained from the torque evaluation. Combining with the results from TEM and AFM, we suspected the local packing of both chitosans might reduce the crosslink of ENR.

It is important to note that the ENR/RCS nanocomposites give the lower crosslink density as compared to ENR/CSN nanocomposites. This also supported our speculation in the TEM micrographs of which the interaction of RCS and ENR was very low resulting in the remove during TEM sample preparation.

However, when the addition of CSN or RCS was as high as 20 phr, the crosslink density is improved. The fact that the ENR contents in the nanocomposites are lower than that of the neat ENR one, the crosslink density observed was, in other words, an apparent crosslink density. The crosslink density of ENR/CSN and ENR/RCS at 20 phr content implies the effective reinforcement of chitosan matrices.

Table 5.1 Crosslink density (η_{phys}) of ENR nanocomposites

Sample	η_{phys} (mol/cm ³)
ENR	1.86×10^{-4}
ENR/2.5CSN	1.38×10^{-4}
ENR/5CSN	1.20×10^{-4}
ENR/10CSN	1.24×10^{-4}
ENR/20CSN	2.05×10^{-4}
ENR/2.5RCS	1.22×10^{-4}
ENR/5RCS	8.27×10^{-5}
ENR/10RCS	1.01×10^{-4}
ENR/20RCS	1.77×10^{-4}

5.4.7 Hardness

According to the result from AFM analysis, the hardness property was carried out in order to confirm the harder surface of ENR nanocomposites which was obtained after incorporating with CSN and RCS. Figure 5.11A shows the hardness related to CSN and RCS content. The hardness increases as a function of CSN and RCS content as compared to ENR. When the contents of CSN and RCS are above 10 phr, the hardness increases significantly. At 20 phr, the hardness increases for 30-40 %. This reflects the function of CSN and RCS. In all cases, the ENR/CSN nanocomposites show the more significant hardness than those of ENR/RCS. Considering the differences in morphology, we suspect the nanoscaffold structure might function as reinforcing network. This is related to the result from AFM analysis.

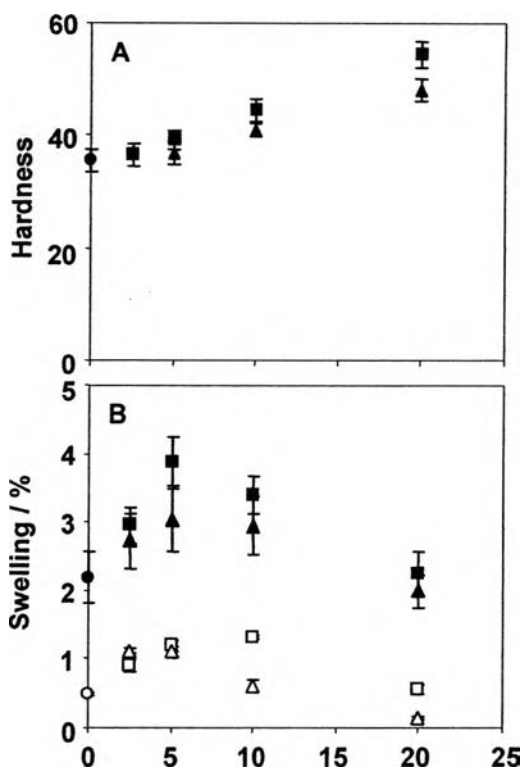


Figure 5.11. (A) Hardness properties of ENR (●) and ENR incorporating with CSN (■), and RCS (▲) and (B) swelling percentage in toluene (solid) and methanol (blank) 24 h of ENR (●) and ENR incorporating with CSN (■) and RCS (▲).

5.4.8 Swelling behavior

The swelling of ENR nanocomposites was observed to evaluate how much CSN and RCS play the role in swelling resistance. The swelling under toluene is a good indicator to show how the fillers protect rubber matrices in swelling. John et al. reported how sisal and oil palm fibers prevented the swelling of NR.³⁴ Okwu et al. reported the swelling of isoprene units of ENR rubber chain based on the toluene swelling.³⁵ As chitosan also swells in rather polar solvents especially acids, here the swellings under toluene and methanol were carried out.

Figure 5.11B shows an increase in the swelling after incorporating with CSN or RCS from 2.5 to 10 phr. The increase in swelling might come from both of the crosslink reduction and the local packing of CSN and RCS to result in phase separation in the nanocomposites. However, the swelling percentage in toluene

decreases after the content of CSN and RCS are at 20 phr. This implied a certain content required for being a good swelling barrier for CSN and RCS.

For methanol swelling, a similar trend was observed. The results reflect the swelling of chitosan in methanol. At 10 phr content, although it is not clear why CSN shows higher swelling than that of RCS, this content seems to be a critical point where the swelling becomes less. The content of 20 phr shows significant swelling barrier which brings the ENR nanocomposites become less swelling than that of the neat ENR system.

5.4.9 Mechanical properties

The various ENR compounds were compressed to obtain nanocomposite in sheet form to evaluate the rubber stiffness. The stiffness also reflects the interaction between ENR and CSN or RCS. Teh et al. used the moduli at 100 % and 300 % elongation to evaluate the stiffness.²¹ Figure 5.12A shows two moduli at 100 % and 300 % elongation for ENR/CSN and ENR/RCS nanocomposites.

At 100 % elongation, ENR nanocomposites with both CSN and RCS show that the moduli are slightly lower than that of the neat ENR. A similar trend is also observed in the case of elongation at 300 %. When the contents of CSN and RCS were increased to 20 phr the moduli significantly increase, especially in the case of CSN. The results support (i) the weak interaction and phase separation of CSN and RCS in ENR matrices at the low content (less than 10 phr), (ii) the packing of CSN and RCS at above 10 phr functions as a reinforcing matrices for ENR, and (iii) at appropriate content (i.e. 20 phr), the morphology of nanoscaffold CSN enhances the stiffness more effective than that of RCS. At this high content, the CSN might form a packing structure and function as a network to retard the solvent penetration resulting in minimum swelling percentage as reported by John et al.³⁴

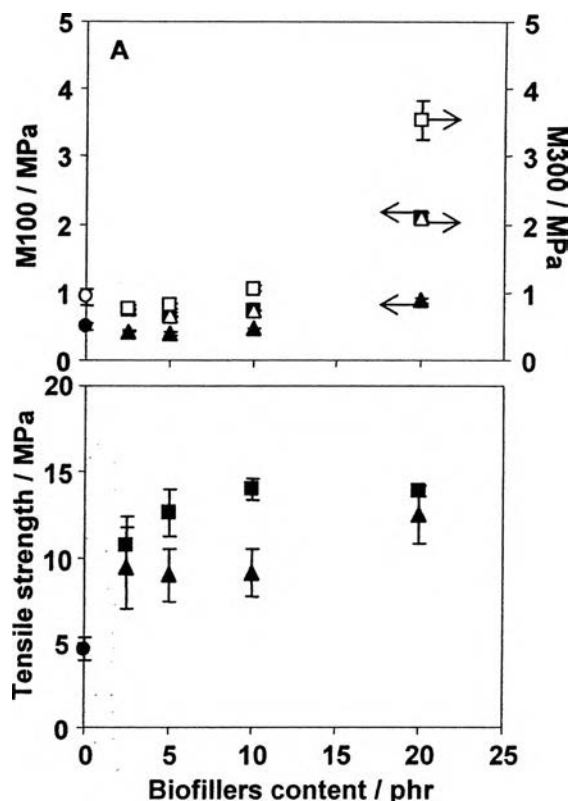


Figure 5.12. (A) Modulus at 100 % elongation (M100) of ENR (●) and ENR nanocomposites with CSN (■) and RCS (▲), and modulus at 300 % elongation (M300) of ENR (○) and ENR nanocomposites with CSN (□) and RCS (△) and (B) tensile strength of ENR (●) and ENR incorporating with either CSN (■) or RCS (▲).

Figure 5.12B shows the tensile strength of ENR and the nanocomposites. All nanocomposites show an improvement of the tensile property. It should be noted that for CSN nanocomposite, the tensile strength increases significantly (more than 200 %) after the content was above 10 phr. Combining with the morphology observed by TEM (Figure 5.2), it can be explained that the high content of CSN might bring the dense packing of CSN resulting in high mechanical properties. In the case of RCS, the increase in tensile strength is significant after the content reaches 20 phr. This reflects a certain local packing of RCS in enhancing the tensile strength.

5.4.10 Tensile fracture surface feature

The SEM technique is an important tool for observing not only morphological feature but also evaluating the interaction between polymer matrices and fillers.³⁴ The fracture surface samples of ENR and ENR nanocomposites were obtained from tensile testing for observing the interaction between chitosans and ENR matrices by using FE-SEM surface analysis. Figure 5.13 shows the FE-SEM micrographs of tensile fracture surface of ENR and ENR incorporating with either CSN or RCS. The ENR without any filler demonstrates the smooth fracture surface as shown in Figure 5.13a. According to the pure ENR, ENR nanocomposites with both chitosans (Figure 5.13b and 5.13c) show the rough tensile fracture surface and fibrous chitosan in nanoscale at the loading of 20 phr. This might come from the interaction of chitosans to ENR matrices inducing the roughness of tensile fracture surface. This observation supported the increase in tensile strength of ENR nanocomposites with CSN and RCS as shown in Figure 5.12B.

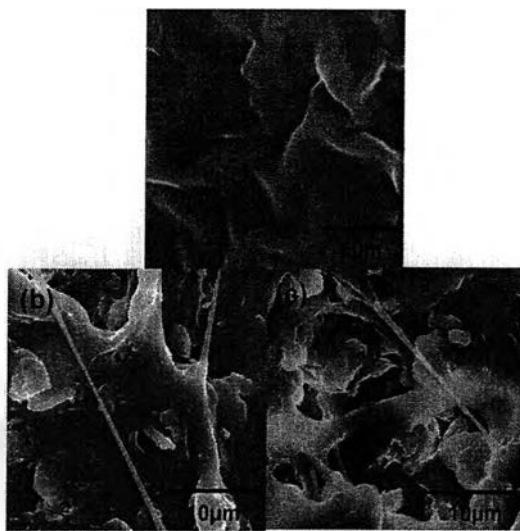


Figure 5.13. FE-SEM micrographs of tensile fracture surface of (a) ENR and ENR nanocomposites with (b) CSN and (c) RCS at 20 phr.

5.5 Conclusion

ENR bio-nanocomposites were prepared by using nano-sized chitosan. Two different morphologies of chitosan, i.e., nanoscaffold (CSN) and reprecipitated nanofiber (RCS) were applied as nano-sized biofillers. The content required for both

chitosans improving the ENR properties in terms of hardness, swelling, and the stiffness was above 10 phr. Although both chitosans tend to form the local packing in ENR, the differences in morphologies between CSN and RCS led us to the conclusion that CSN formed more effective interaction in ENR matrices than RCS. Both nano-sized chitosans demonstrated good performance to adsorb the copper ion. At that time, they also became reinforcing agent in ENR matrices. This evidence will be useful for rubber conductive materials.

5.6 Acknowledgment

The authors (SC and TL) gratefully acknowledge SRI Research & Development Ltd. (SRI R&D), Japan and The Petroleum and Petrochemical College, Chulalongkorn University, Thailand for financial support. The authors would like to extend appreciation to the Seafresh Chitosan (Lab) Company Limited, Thailand, for the chitin and chitosan materials, Sumirubber Malaysia SDN. BHD., Malaysia, for epoxidized natural rubber (ENR) latex, Research and Development Center for Thai Rubber Industry, Thailand, for chemicals, and Labtech Company Limited, Thailand, for rubber compounding. Last but not least, the authors would like to acknowledge the Hitachi High-Technologies Corporation for TEM analysis and Assoc. Prof. Sanong Ekgasit and Mr. Prompong Pienpinijtham for AFM analysis.

5.7 References and notes

1. Ishak, Z. A. M.; Bakar, A. A. *Eur. Polym. J.* **1995**, *31*, 259.
2. Nair, K. G.; Dufresne A. *Biomacromolecules*. **2003**, *4*, 657.
3. Nair, K. G.; Dufresne A. *Biomacromolecules*. **2003**, *4*, 666.
4. Mark, J. E.; Erman, B.; Eirich, F. R. *Science and Technology of Rubber*. 2nd ed.; Academic press, Inc: Sandiago, 1994.
5. Jong, L. *Compos. Part A: Appl. S.* **2007**, *38*, 252.
6. Aylón, E.; Murillo, R.; Fernández-Colino, A.; Aranda, A.; García, T.; Callén, M. S.; Mastral, A. M. *J. Anal. Appl. Pyrol.* **2007**, *79*, 210.
7. Paillet, M.; Dufresne, A. *Macromolecules*. **2001**, *34*, 6527.

8. Carvalho, A. J. F.; Job, A. E.; Alves, N.; Curvelo, A. A. S.; Gandini, A. *Carbohydr. Polym.* **2003**, *53*, 95.
9. Lu, Y.; Weng, L.; Zhang, L. *Biomacromolecules.* **2004**, *5*, 1046.
10. Samir, A. S. A. ; Alloin, F. ; Paillet, M.; Dufresne, A. *Macromolecules.* **2004**, *37*, 4313.
11. Zhang, W. ; Zhang, X. ; Liang, M. ; Lu, C. *Compos. Sci. Technol.* **2008**, *68*, 2479.
12. Ismail, H.; Rozman, H. D.; Jaffri, R. M.; Ishak, Z. A. M. *Eur. Polym. J.* **1997**, *33*, 1627.
13. Kvien, I.; Tanem, B. S.; Oksman, K. *Biomacromolecules.* **2005**, *6*, 3160.
14. Phongying, S.; Aiba, S-I.; Chirachanchai, S. *Polymer.* **2007**, *48*, 393.
15. Lertwattanaseri, T.; Ichikawa, N.; Mizoguchi, T.; Tanaka, Y.; Chirachanchai, S. *Carbohydr. Res.* **2009**, *344*, 331.
16. Bhowmick, A. K.; Stephens, H. L. *Handbook of Elastomers*; Marcel dekker, Inc: Newyork and Basel, 1988.
17. Gan, S-N; Hamid, Z. A. *Polymer*, **1997**, *38*, 1953.
18. Bradbury, J. H.; Perera, M. C. S. *Ind. Eng. Chem. Res.* **1988**, *27*, 2196.
19. Varghese, S.; Karger-Kocsis, J.; Gatos, K. G. *Polymer.* **2003**, *44*, 3977.
20. Ismail, H.; Suzaimah, S. *Polym. Test.* **2000**, *19*, 879.
21. Teh, P. L.; Ishak, Z. A. M.; Hashim, A. S.; Karger-Kocsis, J.; Ishiaku, U. S. *Eur. Polym. J.* **2004**, *40*, 2513.
22. Arroyo, M.; López-Manchodo, M. A.; Valentín, J. L.; Carretero, J. *Compos. Sci. Technol.* **2007**, *67*, 1330.
23. Muzzarelli, R. A. A. *Chitin*; Pergamon Press: Oxford, 1977.
24. Degree of deacetylation (%) = $\{1 - [(I_{H-Ac}/3)/(I_{H-2})]\} \times 100 = \{1 - [(0.1994/3)/(2.1336)]\} \times 100 = 96.88 \%$.
25. Degree of deacetylation (%) = $\{1 - [(I_{H-Ac}/3)/(I_{H-2})]\} \times 100 = \{1 - [(0.2151/3)/(0.6877)]\} \times 100 = 89.57 \%$.
26. Bar, G.; Rubin, S.; Parikh, A. N.; Swanson, B. I.; Zawodzinski, T. A. *Langmuir*, **1997**, *13*, 373.
27. Sasaki, K.; Koike, Y.; Azehara, H.; Hokari, H.; Fujihira, M. *Appl. Phys. A-Mater.* **1998**, *66*, 1275.

28. Jeon, I. H.; Kim, H.; Kim, S. G. *Rubber Chem. Technol.* **2003**, *76*, 1.
29. Jourdan, J. S.; Cruchon-Dupeyrat, S. J.; Huan, Y.; Kuo, P. K.; Liu, G. Y. *Langmuir*, **1999**, *15*, 6495.
30. Foschia, R.; Jobin, M. *Proceeding of International Conference on Nanoscience and Technaology ICN&T*; Basel; Switzerland, 2006.
31. Tsukruk, V. V. *Rubber Chem. Technol.* **1997**, *70*, 430.
32. Kurita, K.; Sannun, T.; Iwakura, Y. *J. Appl. Polym. Sci.*, **1979**, *23*, 511.
33. Wu, F-C.; Tseng, R-L.; Juang, R-S. . *Ind. Eng. Chem. Res.* **1999**, *38*, 270.
34. John, M. J.; Francis, B.; Varughese, K. T.; Thomas, S. *Compos. Part A: Appl. S.* **2008**, *39*, 352.
35. Okwu, U. N.; Okieimen, F. E. *Eur. Polym. J.* **2001**, *37*, 2253.

